

# Transverse Oscillations of Longitudinally Stratified Coronal Loops System

N. Fathalian<sup>1</sup> and H. Safari<sup>2</sup>

<sup>1</sup>*Institute for Advanced Studies in Basic Sciences, P. O. Box 45195-1159, Zanjan, Iran*

<sup>2</sup>*Department of Physics, Zanjan University, P. O. Box 45195-313, Zanjan, Iran*

fathalian@iasbs.ac.ir, safari@znu.ac.ir

## ABSTRACT

The collective transverse coronal loop oscillations seem to be detected in the observational studies. In this regard, Luna et al. (2009, ApJ, 692, 1582) modeled the collective kinklike normal modes of several cylindrical loops system using the T-matrix theory.

This paper investigates the effects of longitudinal density stratification along the loop axis, on the collective kinklike modes of system of coronal loops. The coronal loops system is modeled as cylinders of parallel flux tubes, with two ends of each loop at the dense photosphere. The flux tubes are considered as uniform magnetic fields, with stratified density along the loop axis which changes discontinuously at the lateral surface of each cylinder. The MHD equations are reduced to solve a set of two coupled dispersion relations for frequencies and wave numbers, in the presence of stratification parameter. The fundamental and first overtone frequencies and longitudinal wave numbers are computed. The previous results are verified for unstratified coronal loops system.

Finally we would conclude that increased longitudinal density stratification parameter will result in increase of the frequencies. The frequencies ratios, first overtones to fundamentals, are very sensitive functions of density scale height parameter. Therefore, stratification should be included in dynamics of coronal loops systems. For the unstratified coronal loops system, these ratios are the same as monoloop ones.

*Subject headings:* Sun: corona Sun: magnetohydrodynamics(MHD) waves Sun: oscillations

## 1. Introduction

The high-resolution observations of TRACE, SoHO, Yohkoh, etc provided us with detection of coronal waves (e.g., Aschwanden et al. 1999a, b, 2002; Nakariakov et al. 1999; Schrijver & Brown 2000 and Verwichte et al. 2004). Throughout the development of the observations, transverse and longitudinal oscillations have been studied. The coronal seismology techniques allow the information to be extracted from observations of oscillatory phenomena and the results to be interpreted, using theoretical models (e.g., Edwin & Roberts 1983; Roberts et al. 1984; Goossens et al. 1992).

In the recent observational data, periods, phases, damping times, and mode profiles for coronal loops are reported by Verwichte et al. (2004)

and De Moortel & Brady (2007). Expectedly, the results differ from those based on simplified theoretical models. To be more realistic, several features may be added to this simple model, such as the presence of magnetic twist and shells, field-aligned flows, the role of line-tying effects, loop curvature, coronal leakage, etc.

Andries et al. (2005a,b) pointed out the effect of longitudinally density stratification as an important feature on coronal loop model and oscillations. Andries et al. (2005a, b), Donnelly et al. (2006), Dymova & Ruderman (2006), McEwan et al. (2006), Erdélyi, & Verth (2007), Safari et al. (2007), and Ruderman et al. (2008), used the frequencies ratio,  $P_1/P_2$ , as a seismological tool for estimating the solar atmosphere density scale height. Recently, Andries et al. (2009)

and Aschwanden (2009), reviewed the details of this topic.

Another added feature is the collective nature of the oscillations. This idea comes from the bundles or arcades of loops observed in active regions. As observational instances, Schrijver and Brown (2000) observed antiphase transverse oscillations of adjacent loops and Verwichte et al. (2004) reported phase and antiphase motions, in a post-flare arcade. The exact structures of the active regions coronal loops have not been determined yet. Actually, we don't know exactly, whether those structures are monolithic or multistranded. Multistranded model assumes that each loop is composed of miniloops -several tens or hundreds of strands (Klimchuk 2006). In the context of non individual flux tube oscillations, the propagation of fast waves in two slabs (Murawski 1993; Murawski & Roberts 1994), and the oscillations of the prominence threaded structure (Díaz et al. 2005) have been studied.

Gruszecki et al. (2006), considered impulsively generated oscillations in a 2D model of a curved solar coronal arcade loop that consists of up to 5 strands of dense plasma. Pascoe et al. (2007), studied the effect of fine multishell structuring on the resonant periods of global sausage fast MHD oscillations of straight magnetic slab model of coronal loops. They indicated that the resonant properties of long-wavelength sausage standing modes are not sensitive to fine structuring.

Luna et al. (2009), studied the collective kink-like normal modes of loops, which are set with different physical and geometrical properties. They used the scattering theory, T-matrix, as extended by Waterman & Truell (1961) and Ramm (1986). Luna et al. (2009), concluded that loops with similar kink frequencies, oscillate collectively with a frequency slightly different from that of the individual kink mode. Otherwise, a loop with different kink frequency oscillates individually with its own frequency. The kink frequencies of neighboring loops with similar densities are coupled. Luna et al. (2010), investigated the transverse oscillations of a multi-stranded coronal loop, composed of several parallel cylindrical strands. They concluded that, the presumed internal fine structure of a loop influences its transverse oscillations and so presumable multi-stranded coronal loop transverse dynamics cannot be properly described by

those of an equivalent monolithic loop.

Here, we generalize Luna et al. (2009) method to include longitudinal density stratification in collective oscillations of a coronal loops system. We suppose parallel cylindrical flux tubes, with their ends at the photosphere and with a relatively small curvatures. The cylinders are assumed to have no initial material flow, to be pervaded by uniform magnetic fields along their axis, and to have negligible gas pressure (zero- $\beta$  approximation). We use a single PDE equation for  $z$ -component of perturbed magnetic field as derived by Safari et al. (2007), for studying the oscillations of a single isolated longitudinally stratified thin coronal loop. Assuming stratified flux tubes system, the radial and longitudinal parts of this equation are separated. The radial part is solved based on T-matrix theory extended by Luna et al. (2009) and the longitudinal part is investigated similar as Safari et al. (2007). We derive a set of two coupled dispersion relations for oscillations frequencies and longitudinal wave numbers. In the case of unstratified flux tubes system, our approach is similar to that of Luna et al. (2009), which have reduced the MHD equations from the beginning to accommodate system of uniform flux tubes. We calculate the eigenvalues and eigenfunctions of the normal modes of the stratified model.

This paper's layout is as follows: The physical model and the set of two dispersion relations are treated in Secs 2 and 3, respectively. The numerical results and conclusions are presented in Sec. 4.

## 2. Equilibrium model and equations of motions

We use a system of cylindrical coordinates,  $(r, \phi, z)$ . The equilibrium configuration of coronal loops systems is modeled as a set of cylinders with their axis along the  $z$ -coordinate. Each loop characterized as,  $j$ , has the length of  $L$ , radius  $a_j$ , internal density,  $\rho_j(r, \phi, z, \epsilon)$ , and centered at  $\mathbf{r}_j = x_j \mathbf{e}_x + y_j \mathbf{e}_y$ , in  $xy$ -plane, Fig 1. The equilibrium magnetic field is uniform,  $\mathbf{B} = B_0 \mathbf{e}_z$ . The stratified density of each loop,  $j$ , is assumed to be

$$\begin{aligned} \rho_j(r, \phi, z, \epsilon) &= \rho_j(\epsilon) f(\epsilon, z), \quad |\mathbf{r} - \mathbf{r}_j| \leq a_j, \\ &= \rho_0(\epsilon) f(\epsilon, z), \quad \text{for external of loops,} \end{aligned}$$

$$\tilde{\rho} = \frac{\rho_j(\epsilon)}{\rho_j(0)} = \frac{\rho_0(\epsilon)}{\rho_0(0)} = \frac{1}{\int_0^L f(\epsilon, z) dz}, \quad \epsilon = \frac{L}{H} \quad (1)$$

where,  $\epsilon$  is the stratification parameter and  $H$  is the density scale height. The internal and external footpoint densities are  $\rho_j(\epsilon)$  and  $\rho_0(\epsilon)$  for stratified loops and  $\rho_j(0)$  and  $\rho_0(0)$  for unstratified loops. See Safari et al. (2007) and Fathalian et al. (2010).

The set of linearized MHD equations are reduced as a single PDE for  $z$ -component of perturbed magnetic field,  $b_z$ , as

$$\nabla^2 b_z(r, \varphi, z) - \frac{\omega^2}{v_A^2(r, \varphi, z, \epsilon)} b_z(r, \varphi, z) = 0, \quad (2)$$

where,  $v_A = B_0 / \sqrt{4\pi\rho(r, \varphi, z, \epsilon)}$ , the Alfvén velocity, is the step function of  $r$  and  $\varphi$ . Note that, we used Fourier transform for all perturbed quantities,  $\exp(i\omega t)$ . See Safari et al. (2007) for derivation details.

Following as Safari et al. (2007), using Eq. (2) and  $b_z(r, \varphi, z) = \psi(r, \varphi)Z(z)$  we find

$$\nabla_{\perp}^2 \psi^j + k_j^2 \psi^j = 0, \quad j = 1, 2, \dots, N, \quad (3)$$

$$\left(\frac{d^2}{dz^2} - k_j^2\right)Z^j + \frac{\omega^2}{v_{A_j}^2(z, \epsilon)}Z^j = 0, \quad (4)$$

for internal of the loops, in which

$$k_j^2 = \frac{\omega^2}{v_{A_j}^2(z, \epsilon = 0)} - k_z^2, \quad (5)$$

$$\nabla_{\perp}^2 = \frac{1}{r} \frac{\partial}{\partial r} \left( r \frac{\partial}{\partial r} \right) + \frac{1}{r^2} \frac{\partial^2}{\partial \varphi^2},$$

where,  $N$  and  $k_z^2$  are number of loops and a constant, respectively. Similar relations can be obtained for external part of the loops by replacing "j" with "0".

The changes in total pressure should be continuous at the tube lateral surface. On account of the zero- $\beta$  approximation and constancy of equilibrium magnetic field,  $B$ , this reduces to the requirement of the continuity of perturbed magnetic field  $b_z$ . Thus,

$$\begin{aligned} \psi^j(r, \varphi) &= \psi^0(r, \varphi)|_{\mathbf{r}=\mathbf{r}_j+\mathbf{a}_j}, \quad j = 1, 2, \dots, N, \\ Z^j(z) &= Z^0(z)|_{\mathbf{r}=\mathbf{r}_j+\mathbf{a}_j} = Z(z). \end{aligned} \quad (6)$$

Using the boundary conditions, Eq. (6), and

Eq. (3) and (4), containing the equations for external part we get to

$$\frac{d^2 Z}{dz^2} + A\omega^2(\tilde{\rho}f(\epsilon, z) - 1)Z + k_z^2 Z = 0, \quad (7)$$

where the constant  $A$  is defined by,

$$(1 + N)A = \sum_{j=1}^N \frac{1}{v_{A_j}^2(0, z)} + \frac{1}{v_{A_0}^2(0, z)}.$$

Hereafter, we restrict  $z$  to the interval  $[0, L/2]$ , because of symmetry of each loop about its midpoint,  $z = L/2$ . For exponentially stratified plasma,  $f(\epsilon, z) = \exp(-\epsilon z/L)$ . So, the solution of Eq. (7) is:

$$Z(z) = C_1 J_{\nu} \left( \frac{2\tilde{\omega} e^{-\frac{1}{2}\epsilon z}}{\epsilon} \right) + C_2 Y_{\nu} \left( \frac{2\tilde{\omega} e^{-\frac{1}{2}\epsilon z}}{\epsilon} \right), \quad (8)$$

in which  $\nu = -\frac{2\sqrt{\tilde{\omega}^2/\tilde{\rho} - k_z^2}}{\epsilon}$  and  $\tilde{\omega}^2 = A\tilde{\rho}\omega^2$ .

### 3. Dispersion relations

#### 3.1. Dispersion relations of radial part, Eq. (3)

Following Luna et al. (2009), for a system of  $N$  coronal loops, Eq. (3) could be solved by applying T-matrix theory. The T-matrix method states that the net external field is composed of addition of outgoing scattered waves (Bogdan and Cattaneo 1989) and the wave scattered by the  $j$ -th loop is the outcome of a response of the external field minus the contribution of the mentioned loop. The following linear algebraic system of equations for the complex coefficients  $\alpha_m^j$  can be obtained

$$\begin{aligned} \sum_{i \neq j} \sum_{n=-\infty}^{n=\infty} \alpha_n^i T_{nn}^i H_{n-m}^{(1)}(k_0 |\mathbf{r}_j - \mathbf{r}_i|) e^{i(n-m)\varphi_{ji}} \\ + \alpha_m^j = 0, \quad j = 1, \dots, N, \quad m = 1, \dots, m_t, \end{aligned} \quad (9)$$

in which  $\alpha_m^j$  are the expansion coefficient of order  $m$ ,  $k_0$  is the wave number in the external medium,  $|\mathbf{r}_j - \mathbf{r}_i|$  and  $\varphi_{ji}$  are the distance and the angle formed by the center of the  $i$ -th loop with respect to the center of the  $j$ -th loop.  $H_m^{(1)}$  are the Hankel functions of the first kind. The matrix diagonal elements,  $T_{mm}^j$ , of the operator  $T^j$  are

$$\begin{aligned} T_{mm}^j = \\ \frac{k_j^2 k_0 J_m(k_j a_j) J'_m(k_0 a_j) - k_0^2 k_j J'_m(k_j a_j) J_m(k_0 a_j)}{k_0^2 k_j H_m^{(1)}(k_0 a_j) J'_m(k_j a_j) - k_j^2 k_0 H_m^{(1)}(k_0 a_j) J_m(k_j a_j)}. \end{aligned} \quad (10)$$

The sign "′" denotes the derivative of function in respect of argument. For more details see Luna et al. (2009), who have satisfied the continuity of transverse Lagrangian displacement and total pressure at each tube lateral surface to obtain  $T^j$ . The expansion coefficient of order  $m$  of the  $j$ -th loop,  $\alpha_m^j$ , are coupled to all expansion coefficients of the other loops, which reflects the collective nature of the normal modes. For  $N$  loops and  $m_t$  expansion coefficients for each field, there are  $N \times (2m_t + 1)$  equations from Eq. (9), whereas  $m_t$  is the truncation number.

### 3.2. Dispersion relations of longitudinal part, Eq. (8)

The boundary conditions, at footpoint,  $z = 0$ , and apex,  $z = L/2$ , for even and odd modes in the longitudinal direction are

$$Z(z = 0) = Z(z = L/2) = 0, \text{ even modes,} \quad (11)$$

$$Z(z = 0) = Z'(z = L/2) = 0, \text{ odd modes.} \quad (12)$$

Using Eq. (8) and imposing the boundary conditions, Eqs (11) and (12), we can get the following dispersion relations

$$\frac{J_\nu(\alpha e^{-\epsilon/4})}{J_\nu(\alpha)} = \frac{Y_\nu(\alpha e^{-\epsilon/4})}{Y_\nu(\alpha)}, \text{ even modes,} \quad (13)$$

$$\frac{J'_\nu(\alpha e^{-\epsilon/4})}{J_\nu(\alpha)} = \frac{Y'_\nu(\alpha e^{-\epsilon/4})}{Y_\nu(\alpha)}, \text{ odd modes.} \quad (14)$$

$$\alpha = \frac{2\tilde{\omega}}{\epsilon}.$$

Solving the set of equations, Eq. (9) and Eqs (13) and (14), gives the frequency,  $\omega$ , and the wave number,  $k_z$ , simultaneously. Equations (13) and (14) are considered the effect of longitudinal density stratification on collective transverse oscillations, which is directly related to the main goal of the present paper.

## 4. Numerical results and conclusions

### 4.1. Results for two similar loops

The set of Eqs (9), (13), and (14) are solved numerically for  $\omega$  and  $k_z$ , based on trust-region-dogleg algorithm. The dimensionless parameters are, the frequencies,  $\omega L/v_{A1}(\epsilon = 0)$ , the longitudinal wave number,  $Lk_z$ , the tube length scale,  $a/L$ , the separation distance between center of loops,

$d/a$ , the stratification parameter,  $L/H$ , the densities  $\rho_j(\epsilon)/\rho_0(\epsilon)$  and  $\rho_0(\epsilon)/\rho_0(0)$ .

Study the influence of the density on the normal mode properties, we consider a system of two loops with radiuses  $a_1 = a_2 = a = 0.03L$  with their centers separated a distance  $d = 3a$ , along the  $x$  axis. The first loop density is  $\rho_1 = 3\rho_0$  while  $\rho_2$  is changed from  $\rho_2 = 1.1\rho_0$  to  $5\rho_0$ . Just like Luna et al. (2009), we concentrate on the kinklike modes which is the most important mode frequency of transverse oscillations and find four kinklike normal modes named  $P_x$ ,  $AP_y$ ,  $P_y$ , and  $AP_x$ , where  $P$  and  $AP$  refer to phase and antiphase motions of the loops, respectively. In numerical processes, the truncation wave number,  $m_t$ , is cut to  $m = 10$ . Note that in the case of individual loop oscillations, the kink modes are called with  $m = 1$ . Our numerical results, Fig. 2, show that, the discrepancy between  $P_x$  and  $AP_y$ ,  $P_y$  and  $AP_x$ , for stratified and unstratified system of loops is less than 0.01, which verified Luna et al. (2009) results.

In Fig. 2, dimensionless frequencies,  $\omega L/v_{A1}(\epsilon = 0)$ , are plotted versus the second loop density,  $\rho_2/\rho_0$ , and for different density stratification parameter,  $\epsilon$ . As is shown in the figure: a) in the case of unstratified system of coronal loops,  $\epsilon = 0$ , our results are fully in agreement with Luna et al. (2009), (see solid lines), b) as  $\epsilon$  increases the frequencies increase either, more for  $P_y$  and less for  $P_x$  frequencies (dashed lines  $\epsilon = 1$ , dotted lines  $\epsilon = 2$ , and dash-dotted lines  $\epsilon = 3$ ), c) in density contrast, in the case of  $\rho_2 = \rho_1$ , frequencies discrepancy (i.e.,  $P_y - P_x$ ) increases as  $\epsilon$  increases.

Figure 3 shows dimensionless wave numbers,  $Lk_z$ , versus the density of the second loop,  $\rho_2/\rho_0$ , and for different density stratification parameter,  $\epsilon$ . The solid line shows the wave numbers, for phase,  $P_x$  and  $P_y$ , and antiphase,  $AP_x$  and  $AP_y$  modes, for the case of  $\epsilon = 0$ . We see that, the wave numbers of these modes are degenerated, and as  $\epsilon$  increases the degeneracy is broken to two separated branches (for  $P_x$ ,  $AP_y$  and  $P_y$ ,  $AP_x$  modes). Beside that,  $P_x$  and  $AP_y$  ( $P_y$  and  $AP_x$ ) themselves are closely degenerated. Luna et al. (2009) indicated that, the loop length scale (the ratio of loop radius to loop length  $a/L$ ) breaks this degeneracy (see Fig. 3 therein).

In Fig. 4, the first dimensionless overtone frequencies (the first even modes),  $\omega_2 L/v_{A1}(\epsilon = 0)$ , are plotted versus the density of the second loop,

$\rho_2/\rho_0$ , and for different density stratification parameter,  $\epsilon$ . The first overtone frequencies,  $\omega_2$ , increase with increasing of  $\epsilon$  and decrease with increasing  $\rho_2/\rho_0$ . Expectedly, as shown in Figs 2 and 4, for small stratification parameter ( $\epsilon < 3$ ), as  $\epsilon$  increases the first overtone frequencies,  $\omega_2$ , increase more slightly than the fundamental frequencies,  $\omega_1$  (Safari et al. 2007 and Fathalian et al. 2010).

In Fig.5, the ratios of the first overtone frequencies to the fundamental frequencies,  $\omega_2/\omega_1$  (for  $P_x$ ,  $AP_y$  and  $P_y$ ,  $AP_x$  modes) are plotted versus  $\rho_2/\rho_0$  and for different  $\epsilon$ . As was expected, all of the ratios are less than 2 for stratified cases and decreased by increasing  $\epsilon$ . In the case of unstratified system of coronal loops,  $\epsilon = 0$ , the ratios of phase and antiphase frequencies are degenerated. As we see, in the case of  $\epsilon = 0$ , the frequencies ratios don't change with changing of density,  $\rho_2/\rho_0$ . This means that, the frequencies ratios of unstratified system of coronal loops are the same as monoloop ones. As  $\epsilon$  increases this degeneracy is broken to two separated branches (for  $P_x$ ,  $AP_y$  and  $P_y$ ,  $AP_x$ ).

In Fig.6, dimensionless frequencies,  $\omega L/v_{A1}$  ( $\epsilon = 0$ ), and frequencies ratios,  $\omega_2/\omega_1$ , are plotted as a function of  $\epsilon$  and different  $\rho_2$ . The first loop density is  $\rho_1 = 3\rho_0$ . The solid, dashed, and dash-dotted lines are for  $\rho_2 = 1.1\rho_0$ ,  $\rho_2 = 3\rho_0$ , and  $\rho_2 = 5\rho_0$ , for ( $AP_x$ ,  $P_y$ ). Expectedly, in the case of  $\rho_2 = 1.1\rho_0$ , the frequencies ratios,  $\omega_2/\omega_1$ , is close to the monoloop frequencies ratio (solid line, Fig. 6). We see that with increasing of  $\epsilon$  the frequencies increase. Frequencies ratio, in the case of  $\rho_2 = 3\rho_0$ , which is equal to the first loop density, differs from the other ones.

Van Doorsselaere et al. (2007) revisited observational frequencies ratios of Verwichte et al. (2004), to be in the range of  $1.58 \leq \omega_2/\omega_1 \leq 1.82$ . Using Fig. 6, and for typical loop length, 100Mm, corresponding values of the density scale height,  $H = \epsilon^{-1}(L)$ , fall in the range of [38,91]Mm for  $\rho_2 = 1.1\rho_0$ , [36,87]Mm for  $\rho_2 = 5\rho_0$ , and [28,69]Mm for the case of equal density of two loops  $\rho_1 = \rho_2 = 3\rho_0$ . We see that, for a system of two loops with neighboring similar densities, the estimated density scale height changed significantly. Observations with higher resolutions such as Solar Dynamics Observatory could improve the practical values of frequencies ratio. At

that stage, we can compare the effects of different factors (e.g., non-uniform magnetic flux tubes with variable cross sections, system of many loops or multi-strands loops, etc) on the loops dynamics. In the present stage of the three observations, Van Doorsselaere et al. (2007), we can only be encouraged as our expectation of a density scale height is around 50-100 Mm.

## 4.2. Conclusions

In this paper, we extended the study of collective transverse oscillations of system of coronal loops with both radial and longitudinal density stratification. To do this, we composed two different approaches, Luna et al. (2009) approach (used for studying the kinklike oscillations of system of coronal loops) and Safari et al. (2010) approach (applied for studying single isolated stratified coronal loop). Our main results are listed briefly as:

- In the presence of stratification parameter,  $\epsilon$ , we can get dispersion relations (Eqs. 13 and 14), and solve them numerically for the fundamental and first overtone phase and antiphase modes. Similar as Luna et al. (2009), we focused on the collective kinklike oscillations. In stratified system of coronal loops, we see that the frequencies of kinklike normal modes are more or less as kink.
- Density stratification changes the fundamental and first overtone kinklike frequencies and their ratios for systems of two coronal loops. The order of changes for the frequency ratios of two coupled loops in respect of one loop, is about  $\mathcal{O}(10^{-4})$ , and longitudinally stratification has more effect on frequencies ratios with decreasing and degenerating the ratios for phase and antiphase modes.
- The frequencies ratios of unstratified system of coronal loops ( $\epsilon = 0$ ), are the same as for monoloop. Longitudinally density stratification is completely important in dynamics of system of coronal loops, which breaks the existent degeneracy to two separated branches (pairs  $P_x$ ,  $AP_y$  and  $P_y$ ,  $AP_x$ ).

The difficulties in the numerical solutions come from discrimination of different mode numbers

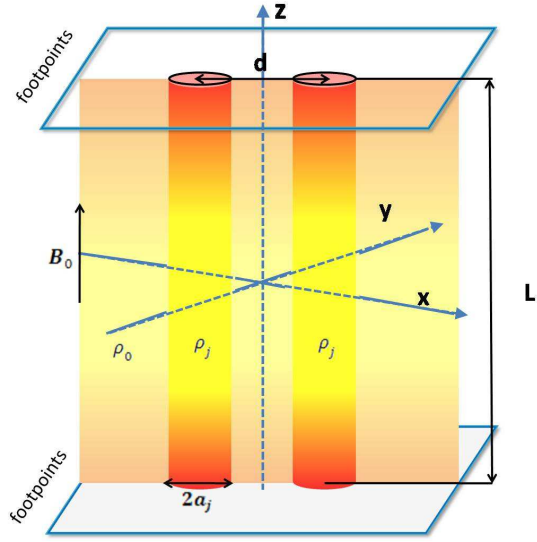


Fig. 1.— A sketch of a system of two straight flux tubes which are presented in the coronal medium. Interior and exterior densities vary along the cylinders axis and are symmetric about the midpoints. The magnetic field is uniform along the  $z$ -axis.

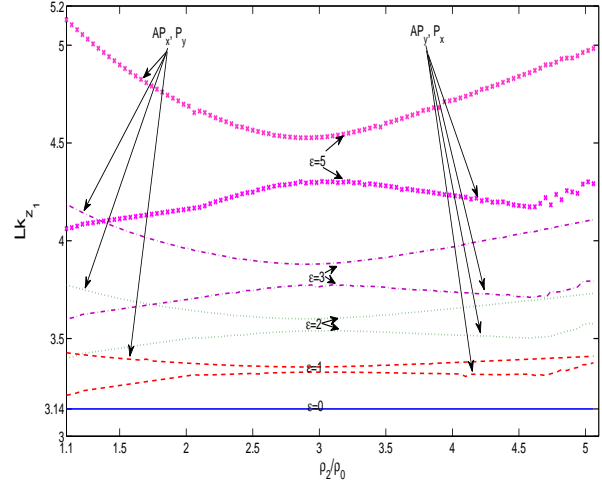


Fig. 3.— Fundamental wave numbers,  $Lk_{z_1}$ , plotted versus  $\rho_2/\rho_0$  and  $\epsilon$  (solid line  $\epsilon = 0$ , dashed lines  $\epsilon = 1$ , dotted lines  $\epsilon = 2$ , dash-dotted lines  $\epsilon = 3$ , and cross lines  $\epsilon = 5$ ).

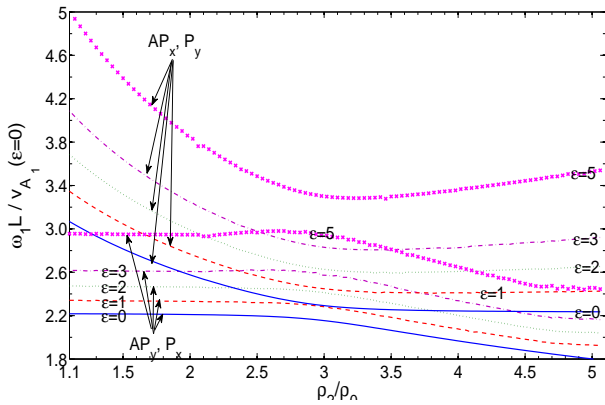


Fig. 2.— The dimensionless fundamental frequencies,  $\omega_1 L/v_{A_1}(\epsilon = 0)$ , plotted versus the density of the second loop,  $\rho_2/\rho_0$ , and for different  $\epsilon$  (solid lines  $\epsilon = 0$ , dashed lines  $\epsilon = 1$ , dotted lines  $\epsilon = 2$ , dash-dotted lines  $\epsilon = 3$ , and cross lines  $\epsilon = 5$ ).

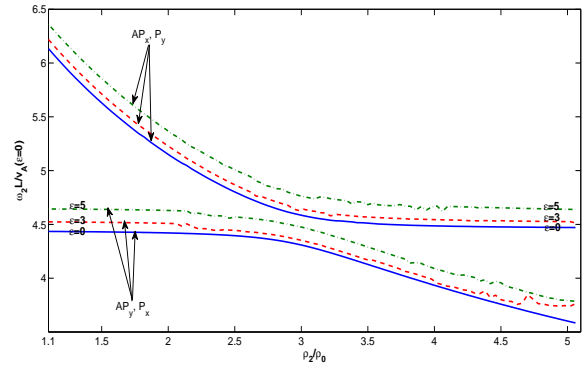


Fig. 4.— The first dimensionless overtone frequencies,  $\omega_2 L/v_{A_1}(\epsilon = 0)$ , plotted versus the density of the second loop,  $\rho_2/\rho_0$ , and for different  $\epsilon$  (solid lines  $\epsilon = 0$ , dashed lines  $\epsilon = 3$ , dash-dotted lines  $\epsilon = 5$ ).

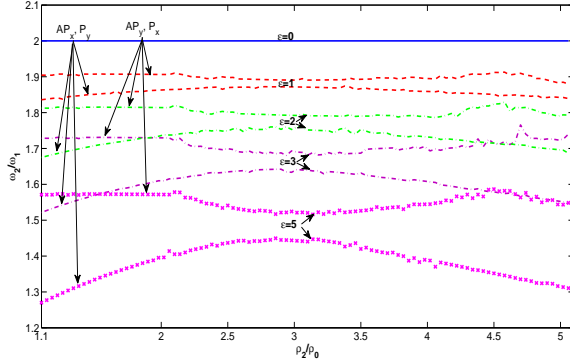


Fig. 5.— The ratios of the first overtone frequencies to the fundamental frequencies,  $\omega_2/\omega_1$ , are plotted versus the density of the second loop,  $\rho_2/\rho_0$ , and for different  $\epsilon$ , for  $P_x$ ,  $AP_y$  and  $P_y$ ,  $AP_x$  modes (solid line  $\epsilon = 0$ , dashed lines  $\epsilon = 1$ , dotted lines  $\epsilon = 2$ , dash-dotted lines  $\epsilon = 3$ , and cross lines  $\epsilon = 5$ ).

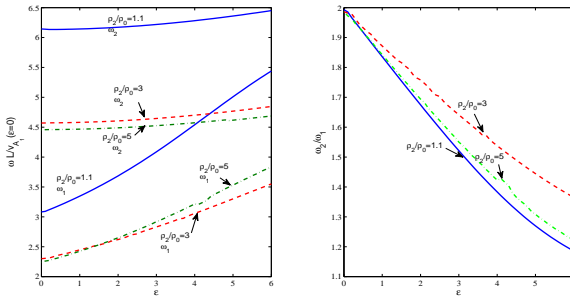


Fig. 6.— The dimensionless frequencies,  $\omega L/v_{A1}$  ( $\epsilon = 0$ ), and the frequencies ratios,  $\omega_2/\omega_1$ , are plotted as a function of  $\epsilon$  and different  $\rho_2$ . The first loop density is  $\rho_1 = 3\rho_0$ . The solid, dashed, and dash-dotted lines are for  $\rho_2 = 1.1\rho_0$ ,  $\rho_2 = 3\rho_0$ , and  $\rho_2 = 5\rho_0$ , for ( $AP_x$ ,  $P_y$ ). We see that with increasing of  $\epsilon$  the frequencies increase expectedly.

with close frequency values. To avoid this, double precision was used in our numerical processes.

## Acknowledgments

The authors would like to thank the unknown referee for his/her very helpful comments and suggestions.

## REFERENCES

- Andries, J., Arregui, I., & Goossens, M. 2005a, *ApJ* 624, L57.
- Andries, J., Goossens, M., Hollweg, J. V., Arregui, I., & Van Doorselaere, T. 2005b, *A&A* 430, 1109.
- Andries, J., Van Doorselaere, T., Roberts, B., Verth, G., Verwichte, E., & Erdélyi, R. 2009, *Space Sci. Rev.*, 149, 3.
- Aschwanden, M. J. 2009, *Space Sci. Rev.*, 149, 31.
- Aschwanden, M. J., De Pontieu, B., Schrijver, C. J., & Title, A. M. 2002, *Sol. Phys.*, 206, 99.
- Aschwanden, M. J., Fletcher, L., Schrijver, C. J., & Alexander, D. 1999a, *ApJ*, 520, 880.
- Aschwanden, M. J., Newmark, J. S., Delaboudinière, J., Neupert, W. M., & Klimchuk, J. A., et al. 1999b, *ApJ*, 515, 842.
- De Moortel, I. & Brady, C. S. 2007, *ApJ*, 664, 1210.
- Díaz, A. J., Oliver, R., & Ballester, J. L. 2005, *A&A*, 440, 1167.
- Donnelly, G. R., Díaz, A. J., & Roberts, B., 2006. *A&A*, 457, 707.
- Dymova, M. V. & Ruderman, M. S. 2006, *A&A*, 459, 241.
- Edwin P. M. & Roberts, B. 1983, *Sol. Phys.*, 88, 179.
- Erdélyi, R. & Verth, G. 2007, *A&A*, 462, 743.
- Fathalian, N., Safari, H., & Nasiri, S. 2010, *New Astronomy*, 15, 403.
- Goossens, M., Hollweg, J. V., & Sakurai, T. 1992, *Sol. Phys.*, 138, 233.

- Gruszecki, M., Murawski, K., Selwa, M., & Ofman, L. 2006, *A&A*, 460, 887.
- Klimchuk, J. A. 2006, *Sol. Phys.*, 234, 41.
- Luna, M., Terradas J., Oliver R., & Ballester J. L. 2009, *ApJ*, 692, 1582.
- Luna, M., Terradas, J., Oliver, R., & Ballester, J. L. 2010, *ApJ*, 716, 1371.
- McEwan, M., Donnelly, G.R., Díaz, A.J., & Roberts, B. 2006, *A&A*, 460, 893.
- Murawski, K. 1993, *Acta Astronomica*, 43, 2, 161.
- Murawski, K. & Roberts, B. 1994, *Sol. Phys.*, 151, 305.
- Nakariakov, V. M., Ofman, L., DeLuca, E. E., Roberts, B., & Davila, J. M. 1999, *Science*, 285, 862.
- Pascoe, D. J., Nakariakov, V. M., & Arber, T. D. 2007, *Sol. Phys.*, 246, 165.
- Ramm, A. G. 1986, *Scattering by obstacles* (Dordrecht: Reidel).
- Roberts, B., Edwin, P. M., & Benz, A. O. 1984, *ApJ*, 279, 857.
- Ruderman, M.S., Verth, G., & Erdélyi, R. 2008, *ApJ*, 686, 694.
- Safari, H., Nasiri, S., & Sobouti Y. 2007, *A&A*, 470, 1111.
- Schrijver, C. J. & Brown, D. S. 2000, *ApJ*, 537, L69.
- Van Doorselaere, T., Nakariakov, V. M., & Verwichte, E. 2007, *A&A*, 473, 959.
- Verwichte, E., Nakariakov, V. M., Ofman, L., & Deluca, E. E. 2004, *Sol. Phys.*, 223, 77.
- Waterman, P. C. & Truell, R. 1961, *JMP*, 2, 512.